Empirical Force Fields for Biologically Active Divalent Metal Cations in Water†

C. Satheesan Babu*,‡ and Carmay Lim*,‡,§

Institute of Biomedical Sciences, Academia Sinica, Taipei 115, Taiwan and Department of Chemistry, National Tsing Hua University, Hsinchu 300, Taiwan

Received: July 28, 2005; In Final Form: October 6, 2005

We have presented a strategy for deriving ion−water van der Waals (vdW) parameters that implicitly include the microscopic solvent molecular effects around the ion. The strategy can be used to obtain vdW parameters for metal cations of the same formal charge and known experimental hydration free energies. In this work, it was applied to derive the vdW parameters for 24 divalent metal ions with measured hydration free energies ranging from −300 to −572 kcal/mol, coordination numbers (CNs) from 4 to 15, and ion−O (water) distances from 1.67 to 2.90 Å. The strategy used to derive the vdW parameters employs (1) a numerical procedure that links the coupling parameter used in free energy simulations with the experimental hydration free energies and (2) the first-shell CNs and structure for the entire series of divalent cations. One of the parameter sets obtained (referred to as MWc) simultaneously reproduces the observed (i) relative hydration free energies, (ii) first-shell CNs, and (iii) average ion−water distances of all the dications studied. In particular, the MWc parameters reproduce the observed (i) decrease in the CN from 6 for Cu^{2+} to 4 for Be^{2+}, (ii) no change in the CN of 6 for dications with hydration free energies between those of Cu^{2+} and Cd^{2+}, and (iii) an expansion of the CN from 6 for Cd^{2+} to 9.5 for Ba^{2+}. The ion−water parameters derived herein represent a first step in the simulations of metalloproteins, which will also require potential energy functions incorporating polarizability, charge transfer, and other electronic effects to accurately model the protein−metal interactions in aqueous solution.

Introduction

Divalent metal cations play important roles in biology and medicine. For instance, Zn(II), Mg(II), and Mn(II) are essential cofactors for many enzymatic reactions catalyzed by nucleases, transferases, and peptidases.[1−6] Other metals such as Cu(II) and Fe(II), owing to their special electronic properties and their ability to exist in more than one oxidation state, are key components of electron-transfer proteins that govern important processes such as photosynthesis and respiration.[7] On the other hand, metals such as Zn(II) and Ca(II) assist in biological function(s) by stabilizing proteins that are involved in gene regulation and signal transduction.[4,8−10] Computer simulations of metalloproteins could help to unravel their structure−function relationships. However, such studies have generally been limited by the lack of accurate force fields, i.e., the potential energy function (PEF) and its associated parameters modeling the interaction of the metal ion of interest with water and biological ligands. Thus, as a first step, we have developed a general strategy to obtain reliable force fields for metal ions interacting with water molecules by deriving van der Waals (vdW) parameters that are consistent with the experimental structural and thermodynamical properties not only for a specific metal ion or a certain group of metal ions, but for all metal dications whose absolute hydration free energies have been measured. The force fields developed herein provide a starting point for modeling metalloproteins in aqueous solution.

An accurate force field for a metal ion in aqueous solution should capture the electronic effects around the cation, in particular, charge transfer from the ligands to the metal ion and vice versa, as well as electronic polarization and geometrical distortion of the first coordination shell.[11−14] These electronic effects could be incorporated in a classical ion−water force field by directly fitting the ab initio derived ion−water potential energy surface to an appropriate functional form. For example, Zn^{2+}, Ni^{2+}, and Co^{2+}−water PEFs have been obtained by fitting an ab initio hypersurface to an analytical function with ten parameters.[15−17] Such a complicated functional form, however, cannot be easily combined with the "conventional" PEF widely used in biomolecular simulations, which employs 12−6 van der Waals (vdW) and Coulomb energies to describe the nonbonded interactions. On the other hand, molecular dynamics (MD) simulations of various metal ions in water using the "conventional" PEF with empirically derived vdW parameters and a full integer charge on the metal could reproduce the experimentally observed metal CNs and average metal−O (water) distances in aqueous solution.[18−22] The ability of the "conventional" 12−6 vdW and Coulomb PEF to reproduce experimental structural and thermodynamical properties in aqueous solution is probably because charge transfer from water molecules to a given metal ion is less than that from more polarizable amino acid ligands[23] and can therefore be neglected to a first approximation, while some of the polarization energy contributions can implicitly be accounted using a full (as opposed to a reduced) charge on the metal.[24]

An accurate force field for a metal ion in aqueous solution should also capture the bulk and microscopic solvent molecular effects, i.e., electrostriction and dielectric saturation, around the cation.[11,12] Electrostriction is mainly enthalpic in origin and

† Part of the special issue "Donald G. Truhlar Festschrift".

* To whom correspondence should be addressed. E-mail: carmay@gate.sinica.edu.tw. E-mail: babu@ibms.sinica.edu.tw.

‡ Institute of Biomedical Sciences.

§ National Tsing Hua University.

10.1021/jp054177x CCC: $33.50
Published on Web 11/16/2005

arises from the crowding of water molecules around the ion due to the increased electric field from the ion, whereas dielectric saturation is mostly entropic in origin and stems from the immobilization of water molecules around the ion due to increased hydrogen-bonding interactions with the ion and bulk water molecules. One way to incorporate these effects in the metal ion−water force field is to adjust the vdW parameters to reproduce the ion's hydration free energy, which encompasses both enthalpic and entropic hydration effects. This approach has been adopted in deriving the vdW parameters for alkali and alkaline earth metal cations[18,19] as well as certain transition metal ions[20,24] in water by using methods such as free energy perturbation simulations with the "conventional" PEF.

In this work, we implicitly include the microscopic effects around a dication by finding appropriate vdW parameters for its interaction with TIP3P[25] water molecules using two key pieces of experimental information. The first is the hydration free energy of the metal ion relative to that of a reference ion. *Relative* $\Delta\Delta G_{hyd}$ values rather than *absolute* ΔG_{hyd} values are used in this work, because the hydration free energy difference between any two metal cations is more accurate than the respective absolute numbers, which differ depending on the standard state and the value of the proton hydration free energy.[26−28] The second is the first-shell CN and average ion−water distance of a metal ion, as compared to those of the same reference ion. Such relative first-shell structural transitions were not considered in previous derivations of ion−water force fields.[18−20] Ion−water vdW parameters were obtained for 24 divalent ions with known experimental hydration free energies, ΔG_{hyd}^{expt},[28] as summarized in the next section. Note that the parameters were adjusted only for the smallest and largest ions studied (Be^{2+} and Ba^{2+}), while those for the other 22 ions were derived from a numerical procedure that links the coupling parameter used in free energy simulations with the above experimental observables, as described in the Materials and Methods section. Since the parameters have been developed using the "conventional" PEF, they can be easily integrated with the widely used biomolecular force fields such as CHARMM[29] or AMBER.[30]

Materials and Methods

Absolute Free Energies and Structural Properties of Metal Dications. Table 1 lists the experimental thermodynamical and structural data for all divalent ions whose hydration free energies, ΔG_{hyd}^{expt},[28] have been measured. The ions are arranged in increasing ΔG_{hyd}^{expt}, i.e., decreasing magnitude of the ΔG_{hyd}^{expt} from Be^{2+} to Ba^{2+}/Ra^{2+}. In addition to the absolute hydration free energies, Table 1 lists the Pauling ionic radii, R_{ion}, and the Born radii, R_{Born}. The latter values are derived from the Born equation[31] for the solvation free energy, ΔG_{solv}, of a spherical ion of charge Q_{ion} and radius, R_{Born}

$$\Delta G_{solv} = \frac{-Q_{ion}^{2}}{2R_{Born}}\left(1 - \frac{1}{\epsilon}\right) \qquad (1)$$

In eq 1, ϵ is the bulk dielectric constant of the solvent (∼80 for water). Although many molecular interpretations of R_{Born} exist,[32,33] there is a consensus that it is related to the structural properties of the *first* shell.[34−37] Table 1 also lists the first-shell CN and average metal−water oxygen distance, d(M−O), of each dication in water derived from X-ray diffraction. Certain distances and CNs in Table 1 have relatively large uncertainties, because the diffraction data are sensitive to experimental conditions and salt composition.

TABLE 1: Experimental Absolute Hydration Free Energies (ΔG_{hyd}^{expt}), Ionic (R_{ion}) and Born (R_{Born}) Radii, as Well as First-Shell CNs and Ion−Oxygen Distances (d(M−O)) for Divalent Ions in Water

M^{2+}	$-\Delta G_{hyd}^{expt}$ [a] (kcal/mol)	R_{ion} [a] (Å)	R_{Born} [b] (Å)	CN[c]	d(M−O)[d] (Å)
Be^{2+}	572.4	0.45	1.15	4[e]	1.67[e]
Cu^{2+}	480.4	0.73	1.36	6[e]	eq: 1.94−2.10[e] ax: 2.27−2.60[e]
Ni^{2+}	473.2	0.69	1.39	6[e]	2.04−2.15[e]
Pt^{2+}	468.5	0.80	1.40	*f*	*f*
Zn^{2+}	467.3	0.75	1.40	6[e]	2.05[g]
Co^{2+}	457.7	0.75	1.43	6[e]	2.08−2.12[e]
Pd^{2+}	456.5	0.86	1.44	*f*	*f*
Ag^{2+}	445.7	0.89	1.47	*f*	*f*
Cr^{2+}	442.2	0.82	1.48	6[e]	eq: 2.08[e]
Fe^{2+}	439.8	0.78	1.49	6[e]	2.10−2.28[e]
Mg^{2+}	437.4	0.72	1.50	6[e]	2.00−2.12[e]
V^{2+}	436.2	0.79	1.50	*f*	*f*
Mn^{2+}	420.7	0.83	1.56	6[e]	2.18−2.20[e]
Hg^{2+}	420.7	1.02	1.56	6[e]	2.33[e]
Cd^{2+}	419.5	0.95	1.56	6[e]	2.29[e]
Yb^{2+}	360.9	1.02	1.82	*f*	*f*
Ca^{2+}	359.7	1.00	1.82	6−10[h]	2.39−2.46[h]
Sn^{2+}	356.1	0.93	1.84	6[e]	eq: 2.33−2.34[e] ax: 2.38−2.90[e]
Pb^{2+}	340.6	1.18	1.93	*f*	*f*
Eu^{2+}	331.0	1.17	1.98	*f*	*f*
Sr^{2+}	329.8	1.13	1.99	8−15[e]	2.60−2.65[e]
Sm^{2+}	328.6	1.19	2.00	*f*	*f*
Ba^{2+}	298.8	1.36	2.19	9.5[e]	2.90[e]
Ra^{2+}	298.8	1.43	2.19	*f*	*f*

[a] Absolute experimental hydration free energies, ΔG_{hyd}^{expt}, and ionic radii, R_{ion}, from Marcus, 1994.[28] [b] Born radii, R_{Born}, computed from the ΔG_{hyd}^{expt} in column 2 using eq 1 with $\epsilon = 80$. [c] Coordination number from diffraction data. [d] Distance from the ion to the first-shell water oxygen from diffraction data; "eq" and "axial" mean equatorial and axial, respectively. [e] From Ohtaki and Radnai, 1993.[38] [f] Either no structural data from diffraction methods have been reported or the diffraction data are considered to be unreliable by Ohtaki and Radnai, 1993.[38] [g] From Muñoz-Páez, 1995.[40] [h] From Megyes, 2004.[39]

First-Shell Structural Transitions of Metal Dications. The absolute hydration free energies and the corresponding CNs in Table 1 show the following first-shell structural features. In going from Be^{2+}, which has the most negative hydration free energy (−572 kcal/mol) among the dications in Table 1, to Cu^{2+}, which has the next most negative hydration free energy (−480 kcal/mol), there is a large increase in the free energy (of 92 kcal/mol) and Born radius (∼0.2 Å) accompanied by a corresponding increase in the metal CN from 4 to 6. In contrast, ions whose ΔG_{hyd}^{expt} fall between ΔG_{hyd}^{expt} of Cu^{2+} and Cd^{2+} (−420 kcal/mol), i.e., Ni^{2+}, Zn^{2+}, Co^{2+}, Cr^{2+}, Fe^{2+}, Mg^{2+}, Mn^{2+}, and Hg^{2+}, as well as Cd^{2+}, are all hexahydrated with successive ΔG_{hyd} increasing by ≤15 kcal/mol. After Cd^{2+}, the next two dications in Table 1, Yb^{2+} and Ca^{2+}, have similar hydration free energies (361−360 kcal/mol) that are much less negative than the ΔG_{hyd}^{expt} of Cd^{2+} (by ∼60 kcal/mol). The first-shell CN for Yb^{2+} is not known, while that for Ca^{2+} varies from 6 to 10, depending on the water/salt ratio and experimental conditions.[38] Recent X-ray diffraction data indicates a CN of 8 for a 1 M $CaCl_2$ solution with the CN decreasing as the $CaCl_2$ salt concentration increases.[39] Since the Born radius increases from 1.56 Å for Cd^{2+} to 1.82 Å for Yb^{2+}/Ca^{2+}, indicating considerable expansion of the first hydration shell, a CN greater than 6 for Yb^{2+}/Ca^{2+} could be expected in dilute solution where there are enough water molecules to fully solvate the ion. As compared to Ca^{2+}, Sn^{2+} has a slightly smaller $|\Delta G_{hyd}^{expt}|$ (356 kcal/mol) and a slightly larger Born radius (1.84 Å), yet its first-

shell CN is reported to be 6 by 2 experimental studies using a relatively low water/salt molar ratio of 12−17. In contrast to Sn^{2+}, the larger Sr^{2+} and Ba^{2+} possess at least 8 water molecules in the first shell.

Therefore, apart from the experimental relative hydration free energies, the metal−water vdW parameters should also reproduce the following first-shell structural transition features: (1) They should yield a $Cu^{2+} \rightarrow Be^{2+}$ $\Delta\Delta G_{hyd}^{expt}$ of −92 kcal/mol with a corresponding decrease in the CN from 6 for Cu^{2+} to 4 for Be^{2+}. (2) They should reproduce the $Cu^{2+} \rightarrow Cd^{2+}$ $\Delta\Delta G_{hyd}^{expt}$ of +61 kcal/mol with no change in the CN. (3) They should yield a $Cd^{2+} \rightarrow Ba^{2+}$ $\Delta\Delta G_{hyd}^{expt}$ of +121 kcal/mol with an expansion of the CN from 6 for Cd^{2+} to 9.5 for Ba^{2+}. The next section describes how these experimental features were used to derive the ion−water vdW parameters for all the dications in Table 1 except Ra^{2+}, whose ΔG_{hyd}^{expt} is the same as that for Ba^{2+}, but its first-shell structural properties are unknown.

Metal−Water vdW Parameters. The "conventional" 12−6 vdW and Coulomb potential energy, U_{ij}, between atoms i and j separated by a distance r_{ij} is given by

$$U_{ij}(r_{ij}) = \epsilon_{ij}\left[\left(\frac{R_{\min,ij}}{r_{ij}}\right)^{12} - 2\left(\frac{R_{\min,ij}}{r_{ij}}\right)^{6}\right] + \frac{e^2 Q_i Q_j}{r_{ij}} \qquad (2)$$

where ϵ_{ij} is the energy well depth, $R_{\min,ij}$ is the distance at the energy minimum for atoms i and j, Q_i and Q_j are the partial charges on atoms i and j, respectively, and e is the proton charge. Note that $R_{\min,ij}$ is related to the collision diameter, σ_{ij}, by $R_{\min,ij} = 2^{1/6}\sigma_{ij}$. The vdW parameters obey the following combining rules

$$R_{\min,ij} = (R_{\min,ii} + R_{\min,jj})/2 = R_{\min,i} + R_{\min,j} \qquad (3a)$$

$$\epsilon_{ij} = \sqrt{\epsilon_i \epsilon_j} \qquad (3b)$$

For the TIP3P[25] water model used in this work, $\epsilon_O = 0.1521$ kcal/mol, while $R_{\min,O} = 1.7682$ Å. The ϵ_i and $R_{\min,i}$ of each dication i were obtained by the procedure described below. Although the resulting parameters are probably not related to any physical variables such as dispersion energies of the ions and core radii, they implicitly include the microscopic molecular and electronic effects around the dication (see Introduction), whose charge is fixed at +2e.

Deriving Metal−Water vdW Parameters. This involves perturbing a dication M^{2+} to L^{2+} in TIP3P water using a parameter λ to couple the initial and final states such that $\lambda = 0$ corresponds to M^{2+}, while $\lambda = 1$ corresponds to L^{2+}. The total ion−solvent and solvent−solvent potential energy at λ, U_λ, is given by

$$U_\lambda = \lambda U_{L^{2+}} + (1 - \lambda)U_{M^{2+}} \qquad (4)$$

By knowing U_λ, the free energy change for converting M^{2+} to L^{2+} in water can then be computed from[41]

$$\Delta\Delta G_{hydr} = \int_0^\lambda \left(\frac{dU}{d\lambda}\right) d\lambda \qquad (5)$$

Appendix 1 shows that the metal−water vdW parameters for a given dication, X^{2+}, whose measured hydration free energy falls between the M^{2+} and L^{2+} hydration free energies, can be determined by knowing its λ value, the vdW parameters of M^{2+}, L^{2+}, and water, and the experimental hydration free energies of the dications, M^{2+}, L^{2+}, and X^{2+}. Thus, the λ of X^{2+} was determined by first computing the $\Delta\Delta G_{hyd}$ between M^{2+} and L^{2+} using eq 5. Because several sets of Zn^{2+}−water vdW parameters have been used in Zn protein simulations (see Results), we initially used Zn^{2+} as a reference ($\lambda = 0$) and perturbed it to the "end-point" ions, Be^{2+} and Ba^{2+} ($\lambda = 1$), whose vdW parameters were adjusted by trial and error to reproduce the measured hydration free energies of Be^{2+} (±105 kcal/mol) and Ba^{2+} (±169 kcal/mol) relative to that of Zn^{2+} (see Table 1). From a plot of $\Delta\Delta G_{hyd}$ vs λ (see Figure 1), the measured hydration free energy of X^{2+} yields the corresponding λ using a linear interpolation procedure. This λ and the vdW parameters of the initial (Zn^{2+}) and final (Be^{2+} or Ba^{2+}) states, as well as TIP3P water, can then be used in eqs A6 and A7 (Appendix 1) to solve for the vdW parameters for X^{2+} in TIP3P water.

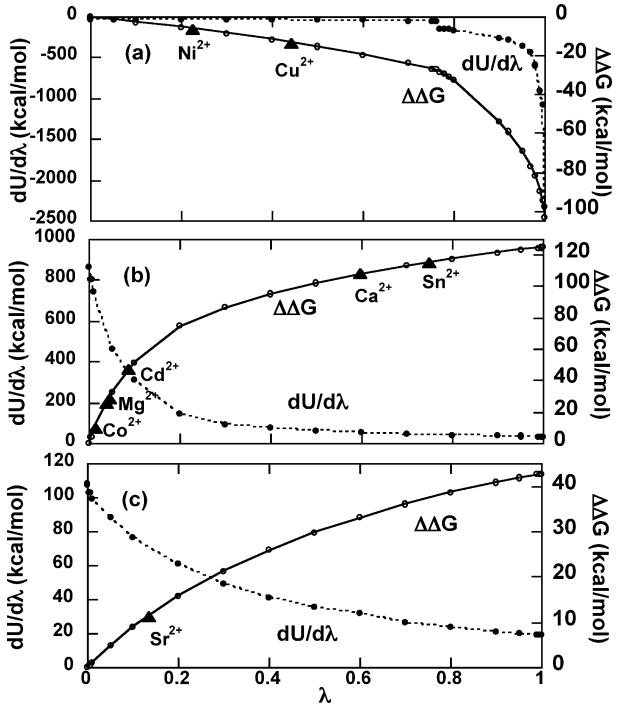

Figure 1. The energy derivative, $dU/d\lambda$ (filled circles, dotted curve), and the corresponding hydration free energy, $\Delta\Delta G_{hyd}$ (open circles, solid line), as a function of the coupling parameter, λ, for the perturbation of (a) Zn^{2+} to Be^{2+}, (b) Zn^{2+} to Pb^{2+}, and (c) Pb^{2+} to Ba^{2+}. The filled triangles correspond to the experimental hydration free energies, $\Delta\Delta G_{hyd}^{expt}$, of some of the dications in Table 1 relative to the corresponding reference ion.

Because the $Zn^{2+} \leftrightarrow Be^{2+}$ and $Zn^{2+} \leftrightarrow Ba^{2+}$ $\Delta\Delta G_{hyd}$ values are large, the initial vdW parameters for X^{2+} were refined to yield the observed first-shell structure and relative free energies of X^{2+}. For example, the $Zn^{2+} \leftrightarrow Ba^{2+}$ perturbation was carried out in two steps: By using the aforementioned procedure, initial vdW parameters for Pb^{2+} were obtained from the $Zn^{2+} \leftrightarrow Ba^{2+}$ perturbation, which were then used to compute the hydration free energy difference between Pb^{2+} and Zn^{2+} (Figure 1b) as well as Pb^{2+} and Ba^{2+} (Figure 1c). The Pb^{2+} and Ba^{2+} vdW parameters were then fine-tuned by hand to reproduce the experimental $\Delta\Delta G_{hyd}$ difference between Pb^{2+} and Ba^{2+}. With the refined Pb^{2+} and Ba^{2+} vdW parameters, the above procedure was again used to obtain refined vdW parameters for the dications lying between Zn^{2+} and Pb^{2+} as well as $Pb^{2+}$and Ba^{2+} in Table 1 (see Results). The resulting vdW parameters were then used in free energy simulations to compute the hydration free energy of each of the dications relative to the reference ion. They were also used in MD simulations of each of the

TABLE 2: vdW Parameters, Hydration Free Energies Relative to Mg^{2+}, and Structural Properties for Zn^{2+} from Previous Works and Experiment

set	ϵ (kcal/mol)	$R_{min}/2$ (Å)	$\Delta\Delta G_{hyd}$ (Zn−Mg) (kcal/mol)	CN	d(Zn−O) (Å)
A[a]	0.183	0.880	−16.0[e]	6	1.95[d]
B[b]	0.250	1.094	+22[e]	6	2.10[d]
expt[c]			−30	6	2.08−2.10

[a] From Sakharov & Lim, 2005.[45] [b] From Stote & Karplus.[20] [c] From Table 1. [d] From the first peak position of the Zn−water oxygen radial distribution function. [e] Using $\epsilon = 0.656$ kcal/mol and $R_{min}/2 = 0.8758$ Å for Mg^{2+} in TIP3P water,[46] which in turn were modified from the values obtained in SPC and TIP3P water.[18,19]

dications in water to compute the ion−oxygen radial distribution functions (rdfs).

Free Energy Perturbation Simulations. The reference ion was placed at the center of a previously equilibrated truncated octahedral box of edge length 55.05 Å containing water molecules at an experimental density of 0.0334 molecules/Å^3. Water molecules whose oxygen atoms were within 2.5 Å of the ion were removed, leaving 2785 water molecules. The solvated ion was first energy-minimized for 1000 steps using steepest descent, followed by 50 ps of equilibration and 100 ps of production dynamics at a mean temperature of 300 K.

The equilibrated ion−water system was then used in the free energy simulations, where the reference ion was perturbed to Be^{2+} or Ba^{2+} using an average of 20 windows between $\lambda = 0$ and $\lambda = 1$. Rather than using equally spaced windows, more windows were constructed in the sharply varying regions of the energy derivative, $dU/d\lambda$, to ensure adequate sampling (see Figure 1). At each window, an equilibrated configuration from the ion−water system was energy-minimized and further equilibrated for 10 ps, followed by 30 ps of production dynamics, during which perturbation energies were stored every 2 fs for computing relative hydration free energies using eq 5. The reverse perturbations were performed from a configuration that is independent from the forward perturbation runs. The free energies for the forward and reverse runs were then averaged.

Simulation Protocol. The simulations were carried out in an *NVE* ensemble using the CHARMM29 program.[42] The bond lengths and angles of TIP3P water molecules were constrained using the SHAKE algorithm.[43] All the simulations employed the leapfrog Verlet integrator with a time step of 2 fs and periodic boundary conditions. The ion−water and water−water nonbonded interactions were truncated using an atom-based force switching function.[44] As relative hydration free energies, as opposed to absolute numbers, were computed, free energy contributions from the long-range electrostatic forces effectively cancel out; therefore, Ewald summation was not employed in the free energy calculations. Instead, a nonbond cutoff of 15 Å was used for all the free energy simulations. For the MD simulations of single ions in water, a much longer cutoff of 22 Å was employed to maximally include the long-range electrostatic forces. Whereas the solvated reference ion was equilibrated for 50 ps followed by 100 ps of production dynamics for use in the free energy perturbation simulations (see above), in the MD simulations each ion−water system was equilibrated up to 100 ps followed by 200 ps of production dynamics, from which the ion−O/H rdfs were computed.

Results

Reference Zn^{2+} vdW Parameters. vdW parameters for the metal dications in Table 1 were obtained using the two Zn^{2+} parameter sets listed in Table 2. The set B Zn^{2+} vdW parameters correspond to those in the CHARMM22 force field.[29] They were based on ϵ_{Zn} and σ_{Zn} obtained initially from fitting to an ab initio derived Zn^{2+}−water potential energy surface and subsequently adjusted to reproduce the experimental first-shell Zn^{2+}−O (water) distance and CN in water (see Table 2), as well as the *absolute* Zn^{2+} ΔG_{hyd}^{expt}.[20] However, the CHARMM Zn^{2+} parameters yield a hydration free energy for Zn^{2+} that is *less* favorable (less negative) than that for Mg^{2+} by 22 kcal/mol (Table 2), whereas experimentally, the Zn^{2+} ΔG_{hyd}^{expt} is *more* favorable than the Mg^{2+} ΔG_{hyd}^{expt} by 30 kcal/mol (see Table 1). The Mg^{2+} parameters used to compute the free energy difference of 22 kcal/mol were taken from ref 46, which in turn were modified from the original values in SPC[18,19] water and TIP3P[35] water (see Table 2 footnote). Furthermore, in MD simulations of the Zn−Cys_2His_2 binding site in a classical Zn-finger domain, the CHARMM Zn^{2+} parameters could not reproduce the experimentally observed tetracoordinated Zn^{2+} but yielded instead Zn^{2+} hexacoordinated to the Cys and His ligands as well as two water molecules.[45]

The set A Zn^{2+} vdW parameters were derived from the Mg^{2+} parameters adapted for TIP3P water (see Table 2, footnotes) by using a similar analytic procedure as in this work to best fit *both* experimental structural and thermodynamical properties of Zn^{2+} in water. They differ from the set B Zn^{2+} vdW parameters in that the Zn^{2+} in set A ($R_{min} = 1.76$ Å) is smaller than that in set B ($R_{min} = 2.18$ Å), but nearly identical in size to the Mg^{2+} ($R_{min} = 1.76$ Å) model used to compute the $\Delta\Delta G_{hyd}$ between Zn^{2+} and Mg^{2+}. They underestimate the experimental Zn^{2+}−O (water) distance (by 0.10 Å) and the magnitude of the hydration free energy difference between Zn^{2+} and Mg^{2+} (by 14 kcal/mol). However, they reproduce the observed first-shell CN and second-shell Zn^{2+}−O (water) distance and yield a hydration free energy for Zn^{2+} that is more negative than that for Mg^{2+}. They also reproduce the observed tetrahedral Zn−Cys_2His_2 geometry in classical Zn-finger domains when charge transfer and polarization effects were explicitly included in the PEF.[45]

vdW Parameters Based on Set A Zn^{2+} Parameters. On the basis of Be^{2+} and Ba^{2+} vdW parameters taken from previous works[35,46] and the set A Zn^{2+} vdW parameters in Table 2, free energy simulations perturbing Zn^{2+} to Be^{2+} and Ba^{2+} were performed (see Figure 1). The Be^{2+} and Ba^{2+} vdW parameters were adjusted by trial and error to reproduce the experimental hydration free energies of Be^{2+} and Ba^{2+} relative to Zn^{2+} (see Table 1) in the free energy simulations. From the $Zn^{2+} \leftrightarrow Be^{2+}$ perturbation (Figure 1a), the vdW parameters for Pt^{2+}, Ni^{2+}, and Cu^{2+}, whose $|\Delta G_{hyd}|$ lie between those of Zn^{2+} and Be^{2+}, were deduced using the procedure described in the Methods section.

Because of the large free energy difference between Zn^{2+} and Ba^{2+} (168.5 kcal/mol, Table 1), the vdW parameters for the ions whose $|\Delta G_{hyd}|$ lie between those of Zn^{2+} and Ba^{2+} were determined as follows. First, a trial set of Pb^{2+} vdW parameters was obtained from the $Zn^{2+} \leftrightarrow Ba^{2+}$ perturbation using eqs A6 and A7 in Appendix 1. The Pb^{2+} and Ba^{2+} vdW parameters were then fine-tuned so that the $Zn^{2+} \leftrightarrow Pb^{2+}$ (Figure 1b) and $Pb^{2+} \leftrightarrow Ba^{2+}$ (Figure 1c) perturbations reproduced the respective experimental $\Delta\Delta G_{hyd}$. The vdW parameters for the ions whose $|\Delta G_{hyd}|$ lie between the Zn^{2+} and Pb^{2+} $|\Delta G_{hyd}|$ were obtained from the $Zn^{2+} \leftrightarrow Pb^{2+}$ perturbation, while those for Eu^{2+}, Sr^{2+}, and Sm^{2+} were derived from the $Pb^{2+} \leftrightarrow Ba^{2+}$ perturbation.

The resulting vdW parameters in Table 3, referred to as MWa, can reproduce the experimental hydration free energies relative

TABLE 3: Computed Hydration Free Energies and Structural Properties of Metal Dications in Water Based on vdW Parameters Derived from Set A Zn^{2+} vdW Parameters[a]

M^{2+}	ϵ (kcal/mol)	$R_{min}/2$ (Å)	$\Delta\Delta G_{hyd}$(M−Zn)[b] (kcal/mol)	CN[c]	d(M−O)[d] (Å)
Be^{2+}	0.0121	0.2384	−103.0 (+2.2)	2	1.23 (−0.44)
Cu^{2+}	0.0734	0.8685	−13.3 (−0.1)	6	1.90
Ni^{2+}	0.1547	0.8783	−6.1 (−0.1)	6	1.95 (−0.09)
Pt^{2+}	0.1752	0.8796	−1.0 (+0.2)	6	1.93
Zn^{2+}	0.1830	0.8800	0.0	6	1.95 (−0.10)
Co^{2+}	0.1226	0.9834	10.0 (+0.4)	6	1.95 (−0.13)
Pd^{2+}	0.1170	0.9959	10.9 (+0.1)	6	1.97
Ag^{2+}	0.0807	1.1009	21.2 (−0.3)	6	2.00
Cr^{2+}	0.0719	1.1360	25.3 (+0.2)	6	2.03
Fe^{2+}	0.0670	1.1578	28.0 (+0.5)	6	2.03 (−0.07)
Mg^{2+}	0.0620	1.1826	29.0 (−0.9)	6	2.03 (0.00)
V^{2+}	0.0596	1.1951	31.1 (+0.0)	6	2.03
Mn^{2+}	0.0409	1.3294	46.3 (−0.3)	6	2.10 (−0.08)
Hg^{2+}	0.0409	1.3295	46.3 (−0.3)	6	2.10 (−0.23)
Cd^{2+}	0.0395	1.3440	47.0 (−0.8)	6	2.13 (−0.16)
Yb^{2+}	0.0273	1.8236	106.3 (−0.1)	8	2.47
Ca^{2+}	0.0278	1.8311	107.8 (+0.2)	8	2.45 (0.00)
Sn^{2+}	0.0294	1.8513	111.5 (+0.4)	8	2.48
Pb^{2+}	0.0403	1.9245	126.3 (−0.4)	8.5	2.60
Eu^{2+}	0.0532	1.9630	135.8 (−0.4)	9	2.65
Sr^{2+}	0.0557	1.9682	137.7 (+0.3)	9	2.65 (0.00)
Sm^{2+}	0.0583	1.9731	138.2 (−0.4)	9	2.68
Ba^{2+}	0.2800	2.0620	171.3 (+2.8)	9.5	2.93 (+0.03)

[a] From Table 2. [b] $\Delta\Delta G_{hyd}$ is the hydration free energy of M^{2+} relative to Zn^{2+} computed using the vdW parameters in columns 2 and 3; the maximum percentage error in the computed $\Delta\Delta G_{hyd}$ from forward and reverse perturbation runs is 1.5%. The number in parentheses equals the computed $\Delta\Delta G_{hyd}$ minus the respective experimental value in Table 1. [c] Obtained from integrating the rdfs. [d] The average ion−oxygen distance, $\langle d(M-O)\rangle$, is computed as the first peak position of the ion−oxygen rdf; the maximum error is ±0.02 Å. The number in parentheses is the minimum difference between the computed and experimental average ion−oxygen distances.

to $\Delta G_{hyd}^{expt}(Zn^{2+})$ to within 3 kcal/mol. They also reproduce the observed CN of 6 for Cu^{2+}, Ni^{2+}, Zn^{2+}, Co^{2+}, Cr^{2+}, Fe^{2+}, Mg^{2+}, Mn^{2+}, Hg^{2+}, and Cd^{2+} and the observed expansion of the CN to 9.5 for Ba^{2+}. However, they underestimate the average first-shell ion−O (water) distance for dications with Born radii smaller than that of Ca^{2+}, especially Be^{2+}, and yield an incorrect CN of 2 for Be^{2+}.

vdW Parameters Based on Set B Zn^{2+} Parameters. On the basis of the set B/CHARMM Zn^{2+} vdW parameters in Table 2, vdW parameters were derived for the dications by adopting the procedure used to derive the MWa parameters in Table 3. The resulting parameters (referred to as MWb) were used in MD and free energy simulations of the dications listed in Table 4. The resulting hydration free energies relative to $\Delta G_{hyd}(Zn^{2+})$ are all close to the respective experimental values. As compared to the MWa parameters, the MWb parameters yield the observed tetracoordination of Be^{2+} and an ion−O (water) distance (1.57 Å) that is closer to the experimental value (1.67 Å).[38,47] They also reproduce the ion−O (water) distances and CNs of ions (Cu^{2+} and Co^{2+}) whose hydration free energies are close to $\Delta G_{hyd}(Zn^{2+})$. However, the MWb parameters greatly overestimate the ion−O (water) distances and CNs of metal dications whose Born radii exceed the Zn^{2+} Born radius by more than 0.05 Å. In particular, they predict the wrong CN of 7 for Mg^{2+} in water, thus predicting an expansion of the CN that is much earlier than observed experimentally (see Table 1).

New Reference Cd^{2+} vdW Parameters. Since the vdW parameters derived from the set B/CHARMM Zn^{2+} parameters could yield the observed structural properties of dications with Born radii of <1.45 Å, but predicted too early an expansion of the CN, we chose Cd^{2+} instead of Zn^{2+} as the new reference state because it is the "largest" dication in terms of the Born radius (Table 1) that has an unambiguous measured CN of 6. We assume that dications with Born radii much larger than that of Cd^{2+}, indicating an expansion of the first shell, have a CN greater than the Cd^{2+} CN, as evidenced by recent X-ray diffraction data[39] suggesting a CN of 8 for Ca^{2+} in water. New vdW parameters were obtained for Cd^{2+} by perturbing it to Ca^{2+} using the MWa parameters in Table 3 and analyzing the hydrated structures between $\lambda = 0.08$ and $\lambda = 0.15$, where the energy derivative, $dU/d\lambda$, varies sharply (Figure 2). Since the structures are hexahydrated when $\lambda \leq 0.1$ but are mainly heptahydrated when $\lambda = 0.15$, a coupling parameter ($\lambda = 0.1$) just before the transition from hexa- to heptahydrated Cd^{2+} was used in eqs A6 and A7 (Appendix 1) to obtain new Cd^{2+} parameters. The latter values, listed in Table 5, yield a hydration free energy that is ∼14 kcal/mol greater than the absolute ΔG_{hyd} obtained using the Cd^{2+} parameters in Table 3. They also yield a Cd−O distance (2.17 Å) between that derived from the MWa (2.13 Å) and MWb (2.38 Å) parameters.

TABLE 4: Computed Hydration Free Energies and Structural Properties of Selected Metal Dications in Water Based on vdW Parameters Derived from Set B/CHARMM Zn^{2+} vdW Parameters[a]

M^{2+}	ϵ (kcal/mol)	$R_{min}/2$ (Å)	$\Delta\Delta G_{hyd}$(M−Zn) (kcal/mol)	CN	d(M−O) (Å)
Be^{2+}	0.2430	0.5274	−103.0 (+2.2)	4	1.57 (−0.10)
Cu^{2+}	0.1305	1.0763	−13.5 (−0.3)	6	2.03
Zn^{2+}	0.2500	1.0944	0.0	6	2.10 (0.05)
Co^{2+}	0.1811	1.1789	9.3 (−0.3)	6	2.12 (0.00)
Mg^{2+}	0.0895	1.3966	29.6 (−0.3)	7	2.24 (0.09)
Mn^{2+}	0.0560	1.5721	46.2 (−0.4)	8	2.39 (0.19)
Cd^{2+}	0.0523	1.5852	47.4 (−0.4)	8	2.38 (0.00)
Ca^{2+}	0.0360	2.1103	106.2 (0.0)	9	2.73 (0.27)

[a] See footnotes under Table 3.

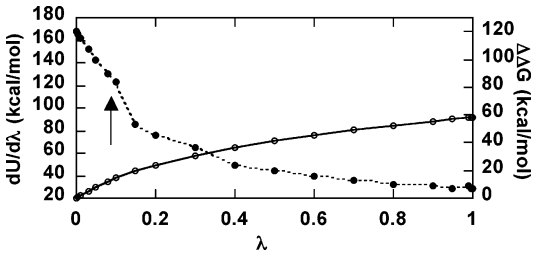

Figure 2. The energy derivative, $dU/d\lambda$ (filled circles, dotted curve), and the corresponding hydration free energy, $\Delta\Delta G_{hyd}$ (open circles, solid curve), as a function of the coupling parameter λ for the perturbation of Cd^{2+} ($\lambda = 0$) to Ca^{2+} ($\lambda = 1$) using the MWa parameters in Table 3. The arrow indicates λ at which the octahedral solvation shell changes to higher-order CNs.

vdW Parameters Based on New Cd^{2+} Parameters. On the basis of the new vdW parameters in Table 5 for Cd^{2+} and MWa parameters in Table 3 for Be^{2+} and Ba^{2+}, free energy simulations perturbing Cd^{2+} to Be^{2+} and Ba^{2+} were performed. The Be^{2+} and Ba^{2+} vdW parameters were adjusted to reproduce the experimental hydration free energies of Be^{2+} and Ba^{2+} relative to Cd^{2+} in the simulations. By using the same procedure to derive the MWa and MWb parameters, vdW parameters for Cu^{2+}, Ni^{2+}, Pt^{2+}, Zn^{2+}, Co^{2+}, Pd^{2+}, Ag^{2+}, Cr^{2+}, Fe^{2+}, Mg^{2+}, V^{2+}, Mn^{2+}, and Hg^{2+} were obtained from the $Cd^{2+} \leftrightarrow Be^{2+}$ perturbation, while those for Yb^{2+}, Ca^{2+}, Sn^{2+}, Eu^{2+}, Sr^{2+}, and Sm^{2+} were derived from the $Cd^{2+} \leftrightarrow Pb^{2+}$ and $Pb^{2+} \leftrightarrow Ba^{2+}$ perturbations. The resulting parameters (referred to as MWc) are listed in Table 5.

TABLE 5: Computed Hydration Free Energies and Structural Properties of Metal Dications in Water Based on vdW Parameters Derived from New Cd^{2+} vdW Parameters[a]

M^{2+}	ϵ (kcal/mol)	$R_{min}/2$ (Å)	$\Delta\Delta G_{hyd}$(M−Cd) (kcal/mol)	CN	d(M−O) (Å)
Be^{2+}	0.0032	0.5637	−156.3 (−3.4)	4	1.57 (−0.10)
Cu^{2+}	0.0427	1.0330	−59.9 (+1.0)	6	1.94
Ni^{2+}	0.0366	1.0941	−53.2 (+0.8)	6	1.97 (−0.07)
Pt^{2+}	0.0332	1.1376	−48.3 (+0.9)	6	1.97
Zn^{2+}	0.0325	1.1489	−47.5 (+0.3)	6	2.00 (−0.05)
Co^{2+}	0.0286	1.2267	−38.0 (+0.2)	6	2.02 (−0.06)
Pd^{2+}	0.0282	1.2360	−37.3 (0.0)	6	2.02
Ag^{2+}	0.0266	1.3107	−26.6 (−0.3)	6	2.06
Cr^{2+}	0.0264	1.3344	−22.4 (+0.7)	6	2.07
Fe^{2+}	0.0264	1.3488	−20.5 (−0.3)	6	2.08 (−0.02)
Mg^{2+}	0.0266	1.3636	−17.5 (+0.9)	6	2.08 (0.00)
V^{2+}	0.0266	1.3706	−16.2 (+0.7)	6	2.11
Mn^{2+}	0.0300	1.4544	−1.5 (−0.2)	6	2.16 (−0.02)
Hg^{2+}	0.0300	1.4544	−1.5 (−0.2)	6	2.16 (−0.17)
Cd^{2+}	0.0304	1.4600	0	6	2.17 (−0.12)
Yb^{2+}	0.0309	1.9298	57.7 (−0.9)	8	2.47
Ca^{2+}	0.0318	1.9364	58.1 (−1.7)	8	2.58 (0.12)
Sn^{2+}	0.0346	1.9540	62.6 (−0.7)	8	2.58
Pb^{2+}	0.0557	2.0195	78.2 (−0.9)	8.5	2.68
Eu^{2+}	0.0647	2.0846	88.8 (+0.4)	9	2.74
Sr^{2+}	0.0664	2.0923	89.3 (−0.3)	9	2.75 (0.10)
Sm^{2+}	0.0680	2.0997	90.1 (−0.7)	9	2.75
Ba^{2+}	0.1993	2.2451	120.4 (−0.3)	9.5	3.01 (0.11)

[a] See footnotes under Table 3.

The MWc parameters in Table 5 can reproduce not only the hydration free energies of all the dications relative to $\Delta G_{hyd}(Cd^{2+})$, but also the structural properties of the ions. The computed relative hydration free energies agree with the respective experimental values to within 1 kcal/mol, except those of Be^{2+} and Ca^{2+}, which deviate from the corresponding experimental numbers by 3.4 and 1.7 kcal/mol, respectively. Note that the absolute ΔG_{hyd} of Zn^{2+} based on the MWc parameters is only 2 kcal/mol less negative than that of the reference Mg^{2+} in Table 2. Furthermore, the MWc parameters reproduce the observed (i) tetrahedral hydration shell of Be^{2+}, (ii) *constant* CN of 6 for Cu^{2+}, Ni^{2+}, Zn^{2+}, Co^{2+}, Cr^{2+}, Fe^{2+}, Mg^{2+}, Mn^{2+}, Hg^{2+}, and Cd^{2+}, and (iii) expansion of the CN from 6 for Cd^{2+} to 9.5 for Ba^{2+}. As compared to the MWa parameters in Table 3, the MWc parameters yield ion−oxygen distances that are closer to the respective experimental values for ions with Born radii smaller than the Born radius of Ca^{2+} (1.82 Å), but not for ions with Born radii much larger than 1.82 Å. Below, we describe the hydration structures derived from MD simulations of the ions using the MWc parameters, as illustrated in Figure 3.

Be^{2+}. The Be^{2+}−O(water) rdf (Figure 3a) shows that the first hydration shell begins at 1.4 Å and ends at 1.8 Å with the first peak centered at 1.57 Å, while the first peak of the Be^{2+}−H(water) rdf is at 2.26 Å (Figure 3b). The first-shell CN of Be^{2+} in water is 4 (Figure 3c), in agreement with experimental data. However, the average $d(Be^{2+}-O)$ distance is shorter than the respective measured value (1.67 Å), while ab initio MD calculations indicate a first-shell peak at 1.65 Å with an rms width of 0.06 Å, in accord with the experimental number.[47] Thus, one possible reason MD simulations with the "conventional" PEF underestimate the observed $d(Be^{2+}-O)$ distance in aqueous solution is that they do not explicitly include the significant nonadditive many-body effects such as distortion of the first-shell water O−H bonds seen in the ab initio MD simulations of Be^{2+} in water.[47]

Cu^{2+}. In analogy to the Be^{2+}−O (water) rdf (Figure 3a), the Cu^{2+}−O (water) rdf also exhibits a first-shell width of 0.4 Å and a difference of ∼0.7 Å between its first peak (1.94 Å) and the first peak of the Cu^{2+}−H (water) rdf (2.65 Å, Figure 3b). The first-shell CN of Cu^{2+} in water is 6 (Figure 3c), in accord with the experimental consensus. On the other hand, ab initio MD simulations support a mixture of 5- and 6-coordinated hydrated structures with a mean Cu^{2+}−O distance of 2.0 Å,[48] but a QM(MP2)/MM simulation study shows a well-defined octahedral shell with a mean Cu^{2+}−O distance of 2.07 Å.[49] The $d(Cu^{2+}-O)$ distance, 1.94 Å, obtained herein is close to the experimental mean of 2.05 Å, obtained by averaging the lower bound of the observed equatorial (1.94 Å) and axial (2.27 Å) distances from Table 1.

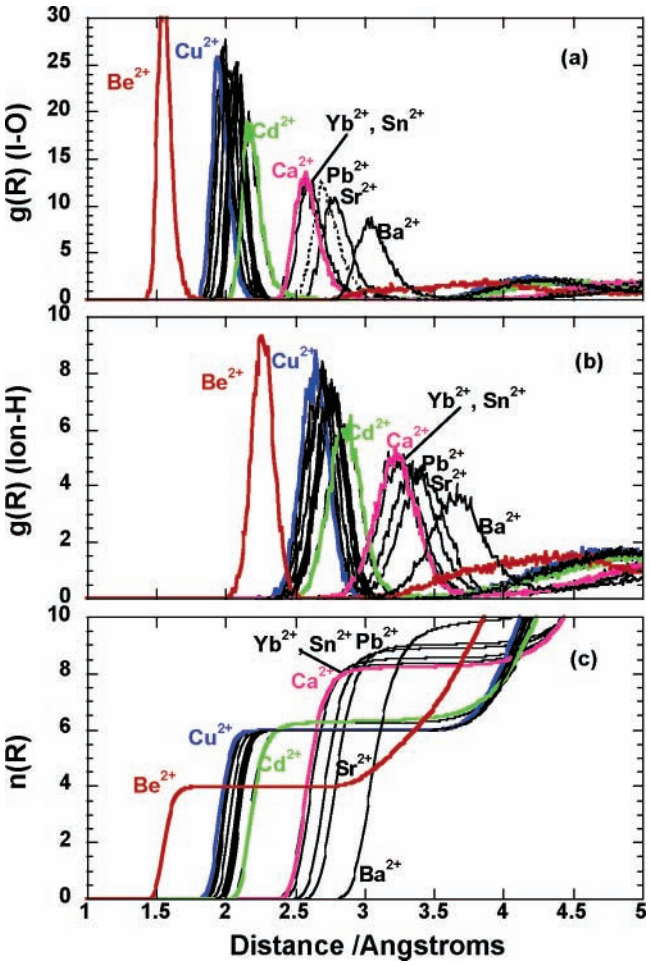

Figure 3. Ion−oxygen rdfs (a), ion−hydrogen rdfs (b), and the corresponding running CNs (c) from 200 ps MD simulations of divalent ions in water using the MWc parameters in Table 5.

Ni^{2+}, Pt^{2+}, Zn^{2+}, Co^{2+}, and Pd^{2+}. These five ions show very stable, octahedral first coordination shells during the 200 ps MD simulations of the ions in water, in accord with the observed first-shell CN of 6 for Ni^{2+}, Zn^{2+}, and Co^{2+}. They are grouped together because they exhibit similar $d(M^{2+}-O)$ values, ranging from 1.97 Å for Ni^{2+} and Pt^{2+} to 2.02 Å for Co^{2+} and Pd^{2+}, as well as similar $d(M^{2+}-H)$ values, ranging from 2.65 Å for Ni^{2+} to 2.70 Å for Pd^{2+}. However, the computed $d(M^{2+}-O)$ distances are shorter than the respective experimental values in Table 1 (by 0.05 to 0.07 Å).

Ag^{2+}, Cr^{2+}, Fe^{2+}, Mg^{2+}, and V^{2+}. As for the previous group of metals, these five ions also show very stable, octahedral shells, in accord with the observed first-shell CN of 6 for these ions except Ag^{2+} and V^{2+}, whose CNs are unknown. They exhibit similar $d(M^{2+}-O)$ values, ranging from 2.06 Å for Ag^{2+} to 2.11 Å for V^{2+}, as well as similar $d(M^{2+}-H)$ values, ranging

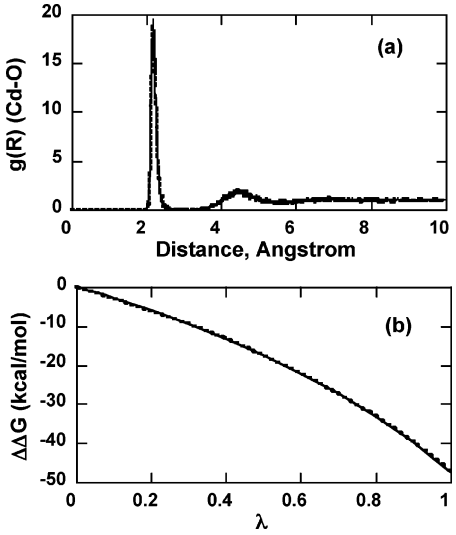

Figure 4. MD and free energy simulations of Cd^{2+} using MWc parameters in TIP3P (solid curve) and SPC/E (dashed curve) water models: (a) $Cd^{2+}-O$ rdfs; (b) solvation free energies for perturbing Cd^{2+} to Zn^{2+} as a function of the coupling parameter λ.

from 2.75 Å for Ag^{2+} to 2.79 Å for V^{2+}. Notably, the computed distances from Cr^{2+}, Fe^{2+}, and Mg^{2+} to the first-shell water oxygen agree with the corresponding measured values.

Mn^{2+}, Hg^{2+}, and Cd^{2+}. These three ions have similar absolute hydration free energies (see Table 1) and thus exhibit similar first-shell hydration structures with a first-shell CN slightly greater than 6 (Figure 3c), $d(M^{2+}-O) = 2.16-2.17$ Å, and $d(M^{2+}-H) = 2.83$ Å. Experimental data indicate a first-shell CN of 6 for Mn^{2+}, Hg^{2+}, and Cd^{2+}, although recent data for Cd^{2+} report CNs of 6 and 7, indicating a Cd^{2+} CN slightly greater than 6.[50,51] Even though the ΔG_{hyd}^{expt} values of Mn^{2+} and Hg^{2+} are identical (−420.7 kcal/mol) and are more negative than that of Cd^{2+} by only 1.2 kcal/mol, the measured $d(M^{2+}-O)$ distances increase in the order $Mn^{2+} < Cd^{2+} < Hg^{2+}$, in contrast to the similar $d(M^{2+}-O)$ predicted for Mn^{2+}, Hg^{2+}, and Cd^{2+}. Consequently, the experimental $d(Cd^{2+}-O)$ and $d(Hg^{2+}-O)$ distances are underestimated in the simulations with the MWc parameters by 0.12 and 0.17 Å, respectively.

Yb^{2+}, Ca^{2+}, and Sn^{2+}. Yb^{2+} and Ca^{2+}, which have very similar hydration free energies, represent the first group of ions among the dications studied with CNs greater than 6. All three ions exhibit a first-shell CN of 8 with $d(M^{2+}-O)/d(M^{2+}-H) = 2.47/3.17$ Å for Yb^{2+} and 2.58/3.22 Å for Ca^{2+} and Sn^{2+}. For Ca^{2+}, the predicted CN is in accord with recent X-ray diffraction data indicating a CN of 8 for 1 M $CaCl_2$ solution.[39] For Sn^{2+}, however, the predicted CN is greater than the reported CN of 6 in two experimental studies, which employed relatively low H_2O/salt molar ratio (<17).[52,53] At this concentration, it is not clear if enough water molecules are available to fully solvate Sn^{2+}; thus, further experimental studies are needed to verify whether the observed CN of 6 corresponds to a fully hydrated Sn^{2+} by determining the metal CN in increasing H_2O/salt molar ratio, i.e., decreasing ion concentration.

Pb^{2+}, Eu^{2+}, Sr^{2+}, and Sm^{2+}. These 4 ions have hydration free energies between those of Sn^{2+} and Ba^{2+}. They exhibit a relatively flexible, expanded coordination shell containing 8.5 to 9 water molecules with $d(M^{2+}-O)/d(M^{2+}-H) = 2.68/3.30$ Å for Pb^{2+} and 2.75/3.40 Å for Eu^{2+}, Sr^{2+}, and Sm^{2+}. The MWc parameters overestimate the $Sr^{2+}-O$ distance (by ∼0.1 Å).

Ba^{2+}. This is the largest of all the divalent ions studied. The first coordination shell of 9.5 water molecules matches the observed CN. However, as for Sr^{2+}, the computed $d(Ba^{2+}-O)$ distance is longer than the corresponding experimental distance by ∼0.1 Å.

Transferability of FF Sets to SPC/E Model of Water. To assess if the ion−water parameters developed here could be directly transferred to other three-site models of water such as the SPC/E model,[54] additional 200 ps simulations of Cd^{2+}, Zn^{2+}, and Ca^{2+} ions in SPC/E water were performed using eq 3 with MWc parameters for the dications and SPC parameters for the water oxygen. The resulting rdfs can be superimposed upon those obtained from the respective simulations using TIP3P water, as illustrated by the $Cd^{2+}-O$ rdf in Figure 4. In addition to the structural similarity, the solvation free energy profile for perturbing Cd^{2+} in SPC/E water as a function of the coupling parameter can be superimposed upon the profile obtained from the respective perturbation in TIP3P water (see Figure 4b), and the hydration free energy of Zn^{2+} relative to that of Cd^{2+} (−47.1 kcal/mol) is very close to the corresponding difference for TIP3P water (−47.5 kcal/mol) in Table 5. The similar solvation structure and thermodynamics obtained in TIP3P and SPC/E water models suggest the transferability of ion−water parameters developed herein to other three-site water models.

Concluding Discussion

We have presented a strategy for deriving ion−water vdW parameters based on currently available structural and thermodynamical properties of dications; this strategy was then used to obtain 3 sets of vdW parameters for 24 dications compatible with three-site water models. All 3 parameter sets reproduce the observed relative hydration free energies (to within 3 kcal/mol). In addition, the MWa parameters in Table 3 predict accurate ion−water structures for relatively big metal ions such as Ca^{2+}, Sr^{2+}, and Ba^{2+}, as well as the observed CNs of nearly all the dications, except the CN of Be^{2+}. The latter may be rectified by including charge transfer and polarization effects[45] (see below) and/or three-body terms[55] in the "conventional" PEF. On the other hand, the MWb parameters in Table 4 can account for the decrease in the CN from 6 for Cu^{2+} to 4 for Be^{2+}, but they predict "too early" an expansion of the first shell, yielding CNs for Mg^{2+}, Mn^{2+}, and Cd^{2+} that are greater than the observed CN of 6. The limitations in the MWa and MWb parameters are corrected in the MWc parameters in Table 5, which reproduce the observed relative first-shell structural transitions, viz., (i) the decrease in the CN from 6 for Cu^{2+} to 4 for Be^{2+}, (ii) no change in the CN of 6 for dications with hydration free energies between those of Cu^{2+} and Cd^{2+}, and (iii) an expansion of the CN from 6 for Cd^{2+} to 9.5 for Ba^{2+}. Thus, the MWc parameters would be suitable for studying the relative properties of divalent cations in water, such as relative binding affinities of metal ions, which require consideration of the desolvation penalty of the metal cation upon binding.

Note, however, that the parameters presented herein are limited by the following factors. The first is the uncertainty in the experimental CN (e.g., Sn^{2+}) and ion−O (water) distances (e.g., Cr^{2+}, Hg^{2+}, Cd^{2+}) of certain cations and the lack of accurate measurements of the CNs and ion−O (water) distances for cations such as Pt^{2+}, Pd^{2+}, Ag^{2+}, V^{2+}, Yb^{2+}, Pb^{2+}, Eu^{2+}, Sm^{2+}, and Ra^{2+} in water. The second limitation in the parameters presented in this work is that they are based solely on structural and thermodynamical properties of the metal ions; they have not taken into account the dynamical properties of the ions or the metal-bound water molecules such as diffusion coefficients and ionic conductivities. Studies on the kinetics of water exchange from the first coordination shell of the metal

ions to the bulk are needed to evaluate the reliability of the MWc parameters in computing dynamical properties. The third limitation is that the force field developed herein do not include ligand−field effects, and therefore, the detailed structure around Jahn−Teller active metals such as Cu^{2+} cannot be reproduced in simulations with the current parameters and the conventional PEF.

The MWa/MWc parameters can be used in combination with current CHARMM/AMBER parameters for simulation studies of metalloproteins in aqueous solution. Indeed, the set A Zn^{2+} vdW parameters have been used in conjunction with the CHARMM force field in MD simulations of a classical Cys_2-His_2 Zn-finger domain and a $Zn-Cys_4$ domain with the "conventional" PEF and a PEF that includes charge transfer and polarization effects.[45] All three factors, viz., charge transfer, local polarization, and appropriate Zn^{2+} vdW parameters, were found to be important in maintaining the structural integrity of the $Zn-Cys_2His_2$ binding site. The importance of appropriate vdW parameters for Zn^{2+} in attaining the correct Zn^{2+} coordination geometry is evidenced from simulations using the "charge transfer + polarization" PEF with the two sets of Zn^{2+} vdW parameters in Table 2. The simulation using the set A Zn^{2+} parameters reproduces the experimentally observed tetrahedral structure of the $Zn-Cys_2His_2$ binding site, even when the simulation started from a nontetrahedral Zn^{2+} configuration. In contrast, the simulation using the set B/CHARMM Zn^{2+} parameters, which are bigger than the set A Zn^{2+} parameters, yields an increase in the Zn−S and Zn−N distances, which, in turn, decreases the amount of charge transferred by the protein ligands to the metal and increases the average Zn charge, as compared to the simulation with the set A Zn^{2+} parameters. This enhances the Zn−water electrostatic interactions to such an extent that the Zn^{2+} is bound to two water molecules in addition to the two Cys^- and two His^0 in the Zn-binding site, yielding a hexacoordinated Zn.

Acknowledgment. C.S.B. is a research fellow of the National Science Council (NSC), Taiwan. This research has been supported by NSC grants 93-2321-B-001-021 (to C.S.B.) and 92-2113-M-001-032 (to C.L.) and the Institute of Biomedical Sciences, Academia Sinica.

Appendix 1

Given the vdW parameters for the "end-point" ions, say Zn^{2+} and Be^{2+}, then the hybrid potential energy at λ corresponding to an ion X^{2+}, e.g., Cu^{2+} or Ni^{2+}, whose $|\Delta G_{hyd}^{expt}|$ falls between the $|\Delta G_{hyd}^{expt}|$ of Zn^{2+} and Be^{2+} could be written according to eq 4 as

$$V_\lambda = \lambda V_{Be^{2+}} + (1-\lambda)V_{Zn^{2+}} \tag{A1}$$

Upon expansion of the solute−solvent potential energy into the r_{ij}^{-12} and r_{ij}^{-6} components

$$V_\lambda = \lambda\sqrt{\epsilon_{Be^{2+}}\epsilon_{OT}}\left[\left(\frac{R_{min,Be^{2+}}+R_{min,OT}}{r_{ij}}\right)^{12} - 2\left(\frac{R_{min,Be^{2+}}+R_{min,OT}}{r_{ij}}\right)^{6}\right] + (1-\lambda)\sqrt{\epsilon_{Zn^{2+}}\epsilon_{OT}} \times \left[\left(\frac{R_{min,Zn^{2+}}+R_{min,OT}}{r_{ij}}\right)^{12} - 2\left(\frac{R_{min,Zn^{2+}}+R_{min,OT}}{r_{ij}}\right)^{6}\right] \tag{A2}$$

where $R_{min,OT}$ and ϵ_{OT} are R_{min} and ϵ parameters for the TIP3P water oxygen, O_T, respectively. Given the experimental $\Delta\Delta G_{hyd}^{expt}$ of X^{2+} from Table 1, the corresponding λ value can be obtained from Figure 1. Thus, the potential energy of X^{2+} whose λ is known can be written as

$$V_{X^{2+}} = \sqrt{\epsilon_{X^{2+}}\epsilon_{OT}}\left[\left(\frac{R_{min,X^{2+}}+R_{min,OT}}{r_{ij}}\right)^{12} - 2\left(\frac{R_{min,X^{2+}}+R_{min,OT}}{r_{ij}}\right)^{6}\right] \tag{A3}$$

Equating the coefficients of r_{ij}^{-12} and r_{ij}^{-6} terms in eqs A2 and A3 yields

$$\sqrt{\epsilon_{X^{2+}}\epsilon_{OT}}(R_{min,X^{2+}}+R_{min,OT})^{12} = \lambda\sqrt{\epsilon_{Be^{2+}}\epsilon_{OT}}(R_{min,Be^{2+}}+R_{min,OT})^{12} + (1-\lambda)\sqrt{\epsilon_{Zn^{2+}}\epsilon_{OT}}(R_{min,Zn^{2+}}+R_{min,OT})^{12} \tag{A4}$$

$$-2\sqrt{\epsilon_{X^{2+}}\epsilon_{OT}}(R_{min,X^{2+}}+R_{min,OT})^{6} = -2\lambda\sqrt{\epsilon_{Be^{2+}}\epsilon_{OT}}(R_{min,Be^{2+}}+R_{min,OT})^{6} - 2(1-\lambda)\sqrt{\epsilon_{Zn^{2+}}\epsilon_{OT}}(R_{min,Zn^{2+}}+R_{min,OT})^{6} \tag{A5}$$

Equations A4 and A5 can be readily solved to yield ϵ and R_{min} of X^{2+} given its λ value.

$$R_{min,X^{2+}} = [(\lambda\sqrt{\epsilon_{Be^{2+}}\epsilon_{OT}}(R_{min,Be^{2+}}+R_{min,OT})^{12} + (1-\lambda)\sqrt{\epsilon_{Zn^{2+}}\epsilon_{OT}}(R_{min,Zn^{2+}}+R_{min,OT})^{12})/(\lambda\sqrt{\epsilon_{Be^{2+}}\epsilon_{OT}}(R_{min,Be^{2+}}+R_{min,OT})^{6} + (1-\lambda)\sqrt{\epsilon_{Zn^{2+}}\epsilon_{OT}}(R_{min,Zn^{2+}}+R_{min,OT})^{6})]^{1/6} - R_{min,OT} \tag{A6}$$

$$\epsilon_{X^{2+}} = \frac{1}{\epsilon_{OT}}[(\lambda\sqrt{\epsilon_{Be^{2+}}\epsilon_{OT}}(R_{min,Be^{2+}}+R_{min,OT})^{6} + (1-\lambda)\sqrt{\epsilon_{Zn^{2+}}\epsilon_{OT}}(R_{min,Zn^{2+}}+R_{min,OT})^{6})/((R_{min,X^{+}}+R_{min,OT})^{6})]^{2} \tag{A7}$$

References and Notes

(1) Berg, J. M. *Annu. Rev. Biophys. Biophys. Chem.* **1990**, *19*, 405−421.
(2) Cowan, J. A. *Biological Chemistry of Magnesium*; VCH: New York, 1995.
(3) Stryer, L. *Biochemistry*, 4th ed.; W. H. Freeman and Co.: New York, 1995.
(4) Lipscomb, W. N.; Strater, N. *Chem. Rev.* **1996**, *96*, 2375−2433.
(5) Holm, R. H.; Kennepohl, P.; Solomon, E. I. *Chem. Rev.* **1996**, *96*, 2239−2314.
(6) Christianson, D. *Prog. Biophys. Mol. Biol.* **1997**, *67*, 217−252.
(7) Lippard, S. J.; Berg, J. M. *Principles of Bioinorganic Chemistry*; University Science Books: Mill Valley, California, 1994.
(8) Coleman, J. E. *Annu. Rev. Biochem.* **1992**, *61*, 897−946.
(9) Forsen, S.; Kordel, J. Calcium in Biological Systems. In *Bioinorganic Chemistry*; Bertini, I., Gray, H. B., Lippard, S. J., Valentine, J. S., Eds.; University Science Books: Mill Valley, California, 1994.
(10) Berridge, M. J.; Bootman, M. D.; Lipp, P. *Nature (London)* **1998**, *395*, 645−648.
(11) Bockris, J. O. M.; Reddy, A. K. N. *Modern Electrochemistry*; Plenum Press: New York, 1977; Vol. 1.
(12) Conway, B. E. *Ionic hydration in chemistry and biophysics*; Elsevier: Amsterdam, 1981.
(13) Cotton, F. A.; Wilkinson, G. *Advanced Inorganic Chemisry*; Jon Wiley & Sons: New York, 1988.
(14) Richens, D. T. *The Chemistry of Aqua Ions*; John Wiley & Sons: New York, 1997.
(15) Marini, G. W.; Texler, N. R.; Rode, B. M. *J. Phys. Chem.* **1996**, *100*, 6808−6813.
(16) Chillemi, G.; D'Angelo, P.; Pavel, N.; Sanna, N.; Barone, V. *J. Am. Chem. Soc.* **2002**, *124*, 1968−1976.
(17) D'Angelo, P.; Barone, V.; Chillemi, G.; Sanna, N.; Meyer-Klaucke, W.; Pavel, N. *J. Am. Chem. Soc.* **2002**, *124*, 1958−1967.
(18) Aqvist, J. *J. Phys. Chem.* **1990**, *94*, 8021−8024.
(19) Aqvist, J. *J. Phys. Chem.* **1994**, *98*, 8253.

(20) Stote, R.; Karplus, M. *Proteins: Struct., Funct., Genet.* **1995**, *23*, 12−31.
(21) Babu, C. S.; Lim, C. *Chem. Phys. Lett.* **1999**, *310*, 225−228.
(22) Yang, P.-K.; Liaw, S.-H.; Lim, C. *J. Phys. Chem. B* **2002**, *106*, 2973−2982.
(23) Dudev, T.; Lim, C. *J. Am. Chem. Soc.* **2002**, *124*, 6759−6766.
(24) Curtiss, L. A.; Halley, J. W.; Hautman, J.; Rahman, A. *J. Chem. Phys.* **1987**, *86*, 2319−2327.
(25) Jorgensen, W. L.; Chandrasekhar, J.; Madura, J. D.; Impey, R. W.; Klein, M. L. *J. Chem. Phys.* **1983**, *79*, 926−923.
(26) Friedman, H. L.; Krishnan, C. V. Thermodynamics of ionic hydration. In *In Water: A comprehensive treatise*; Franks, F., Ed.; Plenum Press: New York, 1973; Vol. 3, pp 1−118.
(27) Marcus, Y. *J. Chem. Soc., Faraday Trans.* **1991**, *87*, 2995−2999.
(28) Marcus, Y. *Biophys. Chem.* **1994**, *51*, 111−127.
(29) MacKerell, J. A. D.; Bashford, D.; Bellott, M.; Dunbrack, R.; Evanseck, J. D.; Field, M. J.; Fischer, S.; Gao, J.; Guo, H.; Ha, S.; Joseph-McCarthy, D.; Kuchnir, L.; Kuczera, K.; Lau, F. T. K.; Mattos, C.; Michnick, S.; Ngo, T.; Nguyen, D. T.; Prodhom, B.; Reiher, W. E. I.; Roux, B.; Schlenkrich, M.; Smith, J. C.; Stote, R.; Straub, J.; Watanabe, M.; Wiorkiewicz-Kuczera, J.; Yin, D.; Karplus, M. *J. Phys. Chem. B.* **1998**, *102*, 3586−3616.
(30) Cornell, W. D.; Cieplak, P.; Bush, B. L. *Comput. Phys. Commun.* **1995**, *91*, 1−4.
(31) Born, M. *Z. Phys.* **1920**, *1*, 45−48.
(32) Latimer, W.; Pitzer, K. S.; Slansky, C. M. *J. Chem. Phys.* **1939**, *7*, 108−111.
(33) Rashin, A. A.; Honig, B. *J. Phys. Chem.* **1985**, *89*, 5588−5593.
(34) Hyun, J.-K.; Ichiye, T. *J. Phys. Chem. B* **1997**, *101*, 3596−3604.
(35) Babu, C. S.; Lim, C. *J. Phys. Chem. B* **1999**, *103*, 7958−7968.
(36) Schmid, R.; Miah, A. M.; Sapunov, N. *Phys. Chem. Chem. Phys.* **1999**, *2*, 97−102.
(37) Ashbaugh, H. S. *J. Phys. Chem. B* **2000**, *104*, 7235−7238.
(38) Ohtaki, H.; Radnai, T. *Chem. Rev.* **1993**, *93*, 1157−1204.
(39) Megyes, T.; Grosz, T.; Radnai, T.; Bako, I.; Palinkas, G. *J. Phys. Chem. A* **2004**, *108*, 7261−7271.
(40) Muñoz-Páez, A.; Pappalardo, R. R.; Marcos, E. *J. Am. Chem. Soc.* **1995**, *117*, 11710−11720.
(41) Beveridge, D. L.; DiCapua, F. M. *Free energy via molecular simulation: A primer*; ESCOM: Leiden, 1989.
(42) Brooks, B. R.; Bruccoleri, R. E.; Olafson, B. D.; States, D. J.; Swaminathan, S.; Karplus, M. *J. Comput. Chem.* **1983**, *4*, 187−217.
(43) Ryckaert, J. P.; Ciccotti, G.; Berendsen, H. J. C. *J. Comput. Phys.* **1977**, *23*, 327.
(44) Steinbach, P. J.; Brooks, B. R. *J. Comput. Chem.* **1994**, *15*, 667−683.
(45) Sakharov, D.; Lim, C. *J. Am. Chem. Soc.* **2005**, *127*, 4921−4929.
(46) Babu, C. S.; Dudev, T.; Casareno, R.; Cowan, J. A.; Lim, C. *J. Am. Chem. Soc.* **2003**, *125*, 9318−9328.
(47) Marx, D.; Sprik, M.; Parrinello, M. *Chem. Phys. Lett.* **1997**, *273*, 360−366.
(48) Pasquarello, A.; Petri, I.; Salmon, P. S.; Parisel, O.; Car, R.; Toth, E.; Powell, D. H.; Fischer, H. E.; Heim, L.; Merbach, A. E. *Science* **2001**, *291*, 856−859.
(49) Schwenk, C. F.; Rode, B. M. *J. Am. Chem. Soc.* **2004**, *126*, 12786−12787.
(50) D'Angelo, P.; Chillemi, G.; Barone, V.; Mancini, G.; Sanna, N.; Persson, I. *J. Phys. Chem. B* **2005**, *109*, 9178−9185.
(51) Chillemi, G.; Barone, V.; D'Angelo, P.; Mancini, G.; Persson, I.; Sanna, N. *J. Phys. Chem. B* **2005**, *109*, 9186−9193.
(52) Yamaguchi, T.; Lindquist, O.; Claeson, T.; Boyce, J. B. *Chem. Phys. Lett.* **1982**, *93*, 528.
(53) Johansson, G.; Ohtaki, H. *Acta Chem. Scand.* **1973**, *27*, 643.
(54) Straatsma, T. P.; Berendsen, H. J. C. *J. Chem. Phys.* **1988**, *89*, 5876.
(55) Probst, M. M.; Spohr, E.; Heinzinger, K. *Chem. Phys. Lett.* **1989**, *161*, 405−408.